JOURNAL OF GEOPHYSICAL RESEARCH VOL. 69, NO. 21 NOVEMBER 1, 1964

Electron Density at the Alouette Orbit

J. O. THOMAS[1] AND A. Y. SADER

Radioscience Laboratory, Stanford University
Stanford, California

Abstract. Alouette topside soundings recorded at Stanford University have been used to determine the diurnal, seasonal, and latitudinal variations of electron density at the orbit of the satellite (~1000 km) over a wide range of latitudes. The electron density is larger in summer than in winter by a factor of approximately 2 at the level of the satellite. The derived latitudinal distributions of electron density at the base of the exosphere are important to the theory of electron and positive ion distributions in the exosphere discussed in the companion paper by Angerami and Thomas.

INTRODUCTION

The satellite monitoring facility operated by the Radioscience Laboratory, Stanford University, has, by special permission of the Canadian Defence Research Telecommunications Establishment and the National Aeronautics and Space Administration, recorded the telemetry signals from the Canadian Topside Sounder 'Alouette' on a routine basis since December 4, 1962. The observational data consist of topside ionograms in which the virtual depth of reflection h' of a radio wave reflected from the topside of the ionosphere is recorded as a function of the variable exploring wave frequency f. The information contained in these ionograms can be used to obtain data about the electron density at the Alouette orbit (approximately 1000 km above the surface of the earth) and the spatial distribution of electrons in the lower exosphere between the peak of the F_2 layer and the satellite.

This paper outlines results obtained from the first series of observations made at Stanford of soundings of the topside of the ionosphere. A technical report containing a detailed account of this work has been published recently [*Thomas and Sader,* 1963] and is available on request to research workers.

Details of the experiments aboard the Alouette satellite have been published in a paper by the *Canadian Defence Research Telecommunications Establishment* [1962]. The first results of the topside sounder experiment carried on the satellite were published by *Warren* [1962] and have been described more fully in a series of papers in the January issue of the *Canadian Journal of Physics,* volume 41, page 188 et seq., 1963, in articles by Warren, Lockwood, Petrie, Hagg, Muldrew, and Nelms. In this paper, details about the satellite and its orbit, the program of observations at Stanford, and the main features of the observed topside ionograms are described. In addition, the diurnal, seasonal, and latitudinal variations of electron density at the orbit of the satellite (~1000 km above the surface of the earth) have been deduced from observations of the extraordinary ray trace. The digital computer program used for data manipulations and calculations is described briefly.

ALOUETTE SATELLITE AND ITS ORBIT

The following information reproduced from the publication of *CDRTE* [1962] relates to the construction, design, and orbital elements of the Alouette satellite, which was launched from the Pacific Missile Range on September 29, 1962.

Mechanical

Shape, oblate spheroid (of spun aluminum).
Diameter, 42 inches.
Height, 34 inches.
Over-all weight, 319 pounds.
Sounding antennas, two crossed dipoles, 150 feet from tip to tip and 75 feet from tip to tip.

[1] Now at Ames Research Center, National Aeronautics and Space Administration, Moffett Field, California.

Telemetry antennas, four whips (turnstile configuration).

Number of solar cells, 6480 arranged in groups of 45.

Batteries, 12 Ni-Cd.

Electrical

Sounding transmitter, completely transistorized.

Frequency sweep, 0.45 to 11.8 Mc/s at approximately 1 Mc/s sec^{-1}.

Pulse width, 100 μsec.

Pulse repetition frequency, 67 cps.

Peak pulse power, 100 watts into 400-ohm load.

Sounding receiver, transistorized.

Frequency sweep, 0.45 to 11.8 Mc/s.

Noise figure, 8 db.

Minimum signal detection through antenna matching networks, 19 db above KTB.

Cosmic noise data provided by AGC voltage.

Beacon transmitter.

Frequency, 136.980 Mc/s at 0.25 watt power.

Frequency, 136.080 Mc/s at 2.0 watts power.

The Alouette orbital elements as computed from Minitrack Observations at NASA Computation Center for September 29, 1962, are given in Table 1.

The telemetry signals are recorded on magnetic tape and subsequently transcribed on to 35-mm film to provide a photographic record of the variation of the virtual depth of reflection beneath the satellite h' as a function of the frequency f of the transmitted radio waves. The topside ionograms are of excellent quality and sweep the range approximately 450 kc/s to 11.8 Mc/s once every 18 sec; during this interval the vehicle travels approximately 120 km. Examples of topside ionograms recorded at Stanford are presented later in the paper.

TABLE 1. Alouette Orbital Elements

Anomalistic period	105.4139 min.
Inclination	80.464°
Mean anomaly	23.754°
Argument of perigee	329.895°
/Motion	−2.566°/day
Latitude of perigee	−29.65°
Right ascension of ascending node	165.773°
/Motion	−0.984°/day
Semimajor axis	$1.15893R_E$
Eccentricity	0.00245
Perigee	618.7 statute miles
Apogee	641.1 statute miles
Velocity at perigee	16467 miles/hour
Velocity at apogee	16387 miles/hour

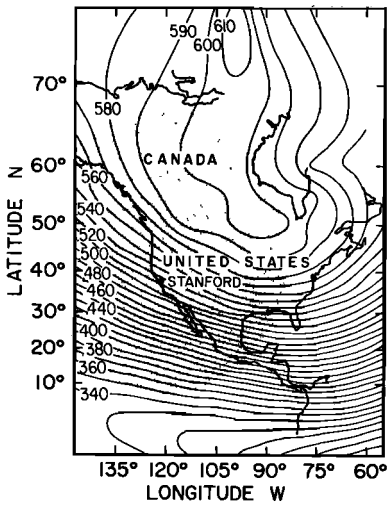

Fig. 1. Position of the telemetry station operated by the Radioscience Laboratory, Stanford University. The dotted area is part of the circular zone in which line-of-sight signals from Alouette are detectable. The variation of the earth's total field is also shown.

Program of Observations at Stanford and Associated Calculations

The location of the receiving site is shown on the map in Figure 1; the dotted area is the major part of the zone in which line-of-sight signals from Alouette are detectable at sufficient strength to obtain good recordings of the topside of the ionosphere. Positional coordinates and magnetic data for Stanford are presented in Table 2. The map (Figure 1) also shows the magnitude of the earth's total magnetic field at the ground. The magnitude of this field at the vehicle, together with the value of the dip angle there, is required in the mathematical analysis for the conversion of the topside $h'(f)$ data into electron density profiles. The procedures used for this purpose have been described elsewhere [*Thomas et al.*, 1963; *Thomas and Westover*, 1963].

TABLE 2. Positional and Magnetic Coordinates of Stanford

Parameter	Value
Geographic latitude	37.43°N
Geographic longitude	122.16°W
Geomagnetic latitude	43.7°N
Dip latitude	45.98°N
Dip angle	64.2°N
Total field	0.515 gauss

To derive information about the electron density in the upper F_2 layer from the observed topside ionograms, it is necessary to know the position of the satellite accurately at the time when the sounding is recorded so that the strength and direction of the earth's field at the location of the vehicle can be determined. The required calculations are described below.

Calculation of geographic latitude and geographic longitude of satellite at a given time. Details about the predicted position of the Alouette satellite are provided regularly by the National Aeronautics and Space Administration in *Alouette Positional Data,* parts 1, 2, and 3, published through NASA Headquarters, Washington, D. C., by Goddard Space Flight Center. Parts 1 and 2 give the time at which the satellite passes above the geographic equator and the longitude at which it crosses the equator, together with the date and pass number for south-north passes. Part 3 gives corrections to be applied to the equatorial crossing data. Thus the information in parts 1, 2, and 3 can be used to determine the satellite's position within the area bounded by the horizon from Stanford. Examples of these predictions were given in Tables 3 and 4 of the paper by *Thomas and Sader* [1963].

Let S (Figure 2*a*) represent the position of Stanford and CSB be the tangent to the earth's surface at S, intersecting the almost circular Alouette orbit at B and C. The angle BOS at the center of the earth is given by

$$\angle BOS = \cos^{-1}(6370/7370) = 30°11'$$

Thus direct line of sight signals cannot be received unless the satellite is at a distance corresponding to less than approximately 30° latitude from Stanford University. From Figure 2*b* it is seen that $\angle SOM = 30°$. Thus

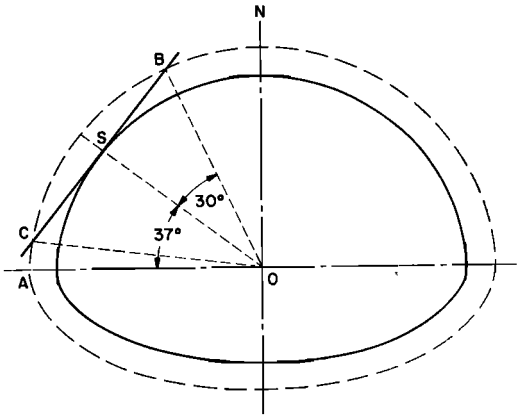

Fig. 2*a*. The intersection of the tangent plane, CSB, through the location of Stanford S, with a concentric sphere 1000 km above the earth.

$$\tan \angle S'OM' = \frac{\tan \angle SOM}{\cos \angle S'OS} = \frac{\tan 30°}{\cos 37°}$$

so that

$$\angle S'OM' = 35°52'$$

From Figures 2*a* and *b* it is seen that the satellite must, if its signals are to be received at Stanford (point S in both figures), lie in an area bounded by a circle of diameter ~7370 km formed by the intersection of the plane tangent to the earth passing through Stanford with a sphere of radius 7370 km. Thus, if it is possible to receive line-of-sight signals from the satellite, the satellite telemetry signals can be received

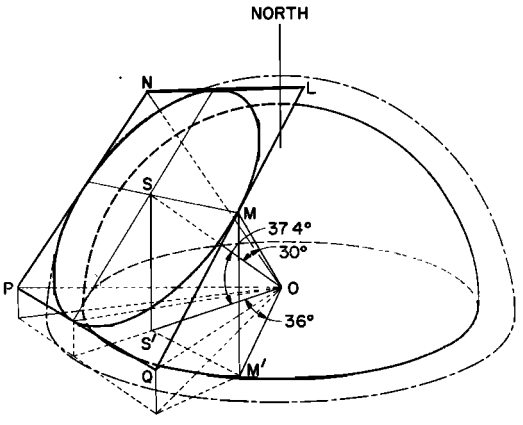

Fig. 2*b*. The intersection of a tangent plane ($LNPQ$) through the location of Stanford S with a concentric sphere 1000 km above the earth.

within the range 37° ± 30° of latitude and 122° ± 36° longitude about the position of Stanford, that is, from 7° to 67° north latitude and from 86° to 158° west longitude. These are the extreme values which the coordinates of the satellite could take, and these extreme values of latitude and longitude could not, of course, be achieved simultaneously. Thus, if a square is plotted of sides corresponding to distances of 122° ± 36°, 37° ± 30°, the longitude and latitude are so related that the satellite's position projected on the tangent plane by a conical projection from the center of the earth will lie inside the circle inscribed in the square *LNPQ* (Figure 2*b*) if its telemetry is to be received at Stanford. The equation of the plane *LNPQ* is

$$\cos\theta\cos\theta_0\cos(\phi-\phi_0)+\sin\theta\sin\theta_0=r/p$$

where θ_0 and ϕ_0 are the geographic latitude and longitude of the point *S*, θ and ϕ are the geographic latitude and longitude west of a point on the plane distance p from the center of the earth, and r is the radius of the earth. The equation of the cone *OCB* (Figure 2*a*) is given by $r/p = \cos 30°$, so that

$$\cos\theta\cos\theta_0\cos(\phi-\phi_0)+\sin\theta\sin\theta_0=\cos 30°$$

For Stanford, $\theta_0 = 37.4°$ and $\phi_0 = 122.2°$.

To determine the position of the satellite at any given time t_0, the following procedure is used. Let the horizontal lines in Figure 3 represent the parallels of latitude drawn 10° apart. Let *AB* represent the direction of a north-south pass and the point *O* represent the position of the satellite at the time t_0. Let *GH* and *IJ* represent the longitudes at which the satellite crosses the parallels *EF* and *CD*, respectively.

Suppose X is the west longitude of the satellite at the time t_0 corresponding to the point *O* in Figure 3, and let

Y = the north latitude of the satellite at the time t_0.
X_1 = the west longitude of the line *GH*.
X_2 = the west longitude of the line *JI*.
Y_1 = the north latitude of the line *EF* crossed at time t_1 just before time t_0.
Y_2 = the north latitude of the line *CD* crossed at time t_2 just after the time t_0.
t_E = time of equatorial crossing.
l_E = longitude of equatorial crossing.

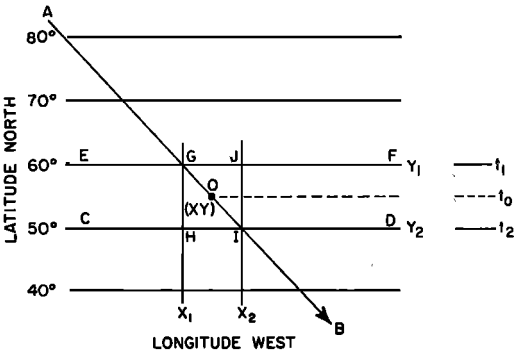

Fig. 3. The determination of the position of the satellite for a north-south pass.

Then

$$Y = Y_1 + \frac{dt}{\Delta t}(Y_2 - Y_1) \qquad (1)$$

$$X = X_1 + \frac{dt}{\Delta t}(X_2 - X_1) \qquad (2)$$

where

$$dt = (t_0 - t_E) - (t_1 - t_E) = t_0 - t_1 \qquad (3)$$

$$\Delta t = t_2 - t_1 \qquad (4)$$

In (1) and (2), $(Y_2 - Y_1)$ and $(X_2 - X_1)$ are computed from the table of corrections to the predictions at the equator crossing, parts 1, 2, and 3 of *Alouette Positional Data*.

For a south-north pass, $(Y_2 - Y_1)$ is positive, as are dt and Δt. The quantity $(dt/\Delta t)(Y_2 - Y_1)$ is added to Y_1 in (1). For a north-south pass, $(Y_2 - Y_1)$ is negative, whereas dt and Δt are still positive. In this case, the correction $(dt/\Delta t)(Y_2 - Y_1)$ is subtracted from Y_1. Similar interpolation gives the value of the west longitude.

The latitudes and longitudes determined from the tables of *Alouette Positional Data* for the crossing points of the 10° latitude-longitude network used for calculating the position of the subsatellite point correspond to projections from the plane of the orbit on to the earth's equatorial plane and on to a meridian plane, respectively. In the calculations described above, linear interpolation in time was used. If the interpolation had been made over the curved path of the Alouette orbit, slightly different and more accurate values of the longitude and lati-

tude of the subsatellite point would have been derived. The magnitude of the error is greater in the computed longitudes than it is for the computed latitudes because of the high inclination of the orbit. The magnitude of the error has been computed in appendix A and is shown to be negligibly small in both cases, so that the linear interpolation used in the calculations is justified.

Once the geographic coordinates of the position of the satellite at the time t_0 are known, it is possible to deduce the magnetic field strength and the dip angle at the location of the satellite.

Derivation of the magnetic parameters at the satellite. The dip angle and gyrofrequency at the satellite can be computed directly from observations of the plasma resonances, gyroresonances, and zero-range echoes which appear on the ionogram [*Lockwood,* 1963; *Calvert and Goe,* 1963], as described in the next section. Alternatively, the dip angle and gyrofrequency can be determined for the exact location of the satellite by extrapolation of ground-based observations of the earth's magnetic field. These quantities can be compared with those derived directly from the ionograms, thus providing an indication of the accuracy of the field model used for the extrapolation from ground-based observations. In practice, it is found that both procedures produce the same result to a high degree of accuracy (see next section).

To determine the dip angle and gyrofrequency for electrons at the subsatellite point (determined by the procedure described in the preceding section), it is necessary to use the best known values for these quantities as measured on the ground. Extrapolations are then made in the manner described below to derive these quantities at the height of the satellite. The magnetic field parameters at the ground are obtained from the *Hydrographic Office* [1954*a*, *b*]. For computation, a grid is constructed on the surface of the earth at intervals of 2° of longitude and latitude in the range 90° to 146° west longitude and 6° to 70° north latitude (Figure 4). The value of the earth's total field F in gauss at each point of this grid is then represented as a matrix stored in the digital computer. The matrix of ground values of the earth's total field and the dip matrix used are given by *Thomas and Sader* [1963, Tables 5 and 6]. The part $ABCD$ of the grid shown in Figure 4 can be approximated by a trapezium which, at latitudes 43° to 45° north, has AB = 157.2 km, $AC = BD$ = 222.4 km, and CD = 162.6 km. In practice, except for very high latitudes, it is sufficiently accurate to regard $ABCD$ as a rectangle, and linear interpolation can be used to determine the magnetic field parameters inside this rectangle. This approximation is justified in appendix B of *Thomas and Sader* [1963], where the lengths of the trapezium sides were calculated for a typical example.

To obtain the field parameters at the vehicle, we first derive the appropriate magnetic parameters for the exact location of the subsatellite point by interpolation in the correct manner within the grid system on the surface of the earth. Once the value of the earth's total field at the appropriate subsatellite point (T, Figure 4) has been determined, an extrapolation involving an inverse cube law is made to derive the corresponding quantity at the vehicle. It is assumed that the dip angle at the satellite has the same value as at the point T on the surface of the earth (Figure 4).

Let (x, y) be the coordinates of the point T on the grid system $ABCD$ (Figure 5), so that

$$x_1 < x < x_2 \qquad y_1 < y < y_2$$

where x_1 and x_2 are consecutive values of the longitude grid lines, and y_1 and y_2 are consecutive values of the latitude grid lines.

In Figure 5 the points $ABCD$ of Figure 4 are re-drawn at the corners of a rectangle instead of a trapezium, and a simple expression, based on a rectangular grid, is first derived for the magnetic field at T. It is then shown (appendix B) that a more accurate derivation, allowing for the curvature of the grid lines, leads to a simple modification of this expression. It was found that the rectangular approximation is, in practice, sufficiently accurate for observations made at Stanford.

Suppose that at the corners of the grid network $ABCD$ the magnetic field parameter concerned (i.e., the total field or the dip angle) has the values shown in Figure 5, so that the total field (or dip angle) takes the values z_1, z_2, and z_3 at the points D, C, and B, respectively.

From Figure 5,

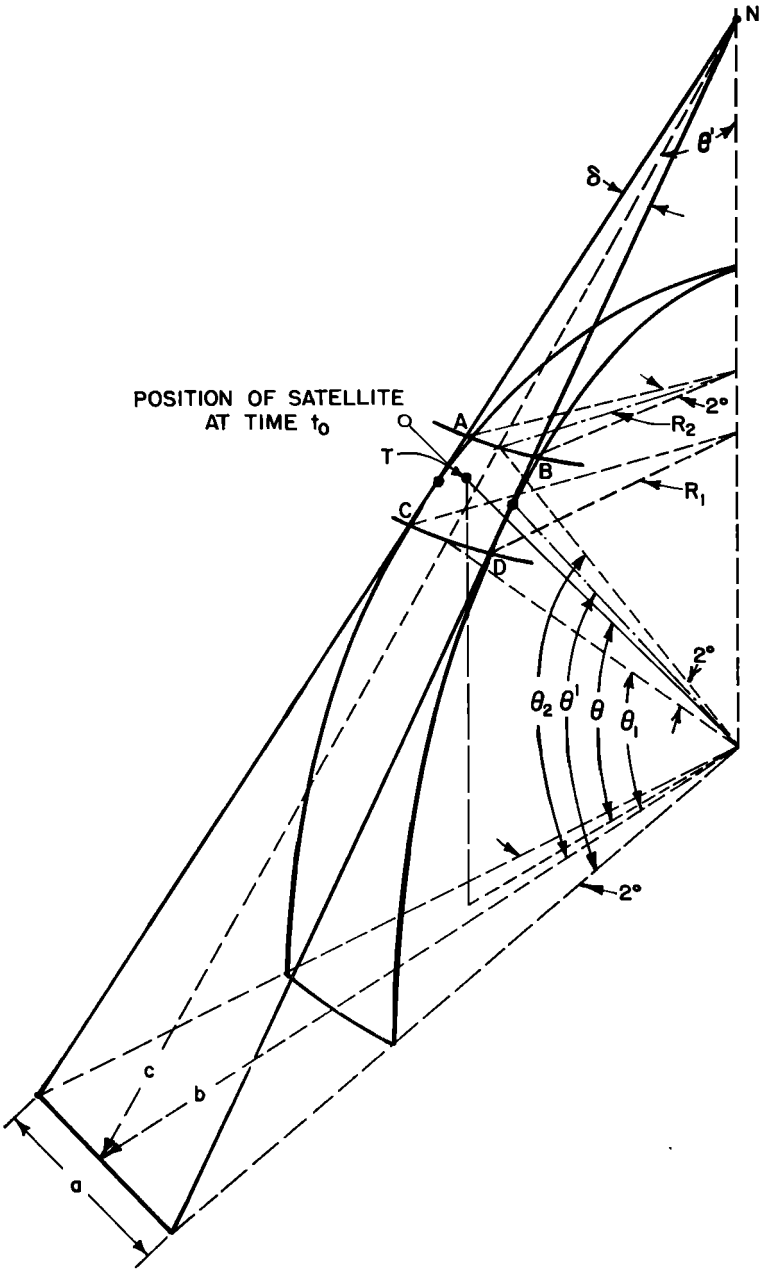

Fig. 4. Convergence of the meridians AC, BD at latitudes between θ_1 and θ_2. The latitude-longitude grid $ABCD$ is used for the determination of the magnetic field parameters at the vehicle.

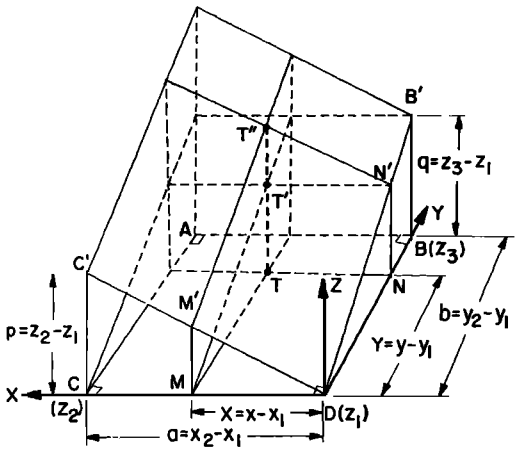

Fig. 5. Calculation of the magnetic field parameters at the subsatellite point T. In this diagram, the points $ABCD$ of Figure 4 are redrawn at the corners of a rectangle.

$$TT'' = TT' + T'T'' = NN' + MM'$$

$$= \frac{X}{a} p + \frac{Y}{b} q$$

X and Y are defined as shown in Figure 5, a and b correspond to the grid spacing (2° in the computations described), and p and q correspond to tabular differences in the magnetic field matrices.

Thus the value of the magnetic field parameter at the subsatellite point T is given by

$$z - z_1 = \frac{(x - x_1)}{(x_2 - x_1)} (z_2 - z_1) + \frac{(y - y_1)}{(y_2 - y_1)} (z_3 - z_1)$$

or

$$z = \frac{X}{a} p + \frac{Y}{b} q + z_1 \qquad (5)$$

In appendix B it is shown that (5) is modified when the curvature of the lines $ABCD$ is allowed for, so that z is given by

$$z = \left(\frac{\cos \theta}{\cos \theta_1}\right) \frac{X}{a} p + \frac{Y}{b} q + z_1 \qquad (6)$$

where θ and θ_1 are the angles shown in Figure 4.

The tabular differences p and q do not exceed 0.015 gauss and θ never exceeds $\theta_1 + 2°$. Hence the error in the computed total field z at T calculated assuming $\cos \theta / \cos \theta_1 = 1$ in (6) does not exceed 0.001 gauss for values of θ up to 86°. In other words, the rectangular grid formula 5 can be used in practice for the analysis of topside ionograms received at Stanford. Indeed, for a grid of spacing 2°, an accuracy of 0.001 gauss in the computed value of z would be obtained even if the tabular differences were as great at 0.05 gauss. In practice, the accuracy limitation arises from the trapezoidal contraction of the longitude meridians as one proceeds from the equator toward the poles. The contraction of meridians was discussed in appendix B of *Thomas and Sader* [1963], where it was shown that the latitude and longitude grid of spacing 2° is, in fact, satisfactory for determining the two magnetic field parameters at the actual location of the satellite if the latitude does not exceed 86° (a latitude never reached by Alouette).

In this section it has been shown how the magnetic parameters at the satellite can be derived from extrapolation of ground-measured values if the position of the satellite at a given time is known accurately. It is possible, however, to deduce the magnitude of the earth's field at the location of the vehicle and also to calculate the value of the dip angle at the satellite from measurements on some of the resonance phenomena which are observed on the ionogram itself. Before the procedures for doing so are outlined, the main features of topside ionograms observed at Stanford are presented and the nomenclature used in their analysis is given.

Calculation of the electron density at the satellite. The main features of a typical daytime ionogram observed at Stanford are presented schematically in Figure 6; traces produced by both the reflected rays and the resonance phenomena are shown. The nomenclature used to describe the main features of these ionograms is shown on the diagram and is detailed in Table 3. The plasma resonance phenomena observed on the Alouette ionograms are not discussed in detail in this report. Relevant magnetoionic conditions which are satisfied by the main resonance phenomena and also by the zero range reflection conditions are summarized in Table 4. Equations 7 to 12 of Table 4 can be solved for the three unknowns X, Y, and θ_v, and hence for f_{Nv}, the plasma frequency at the

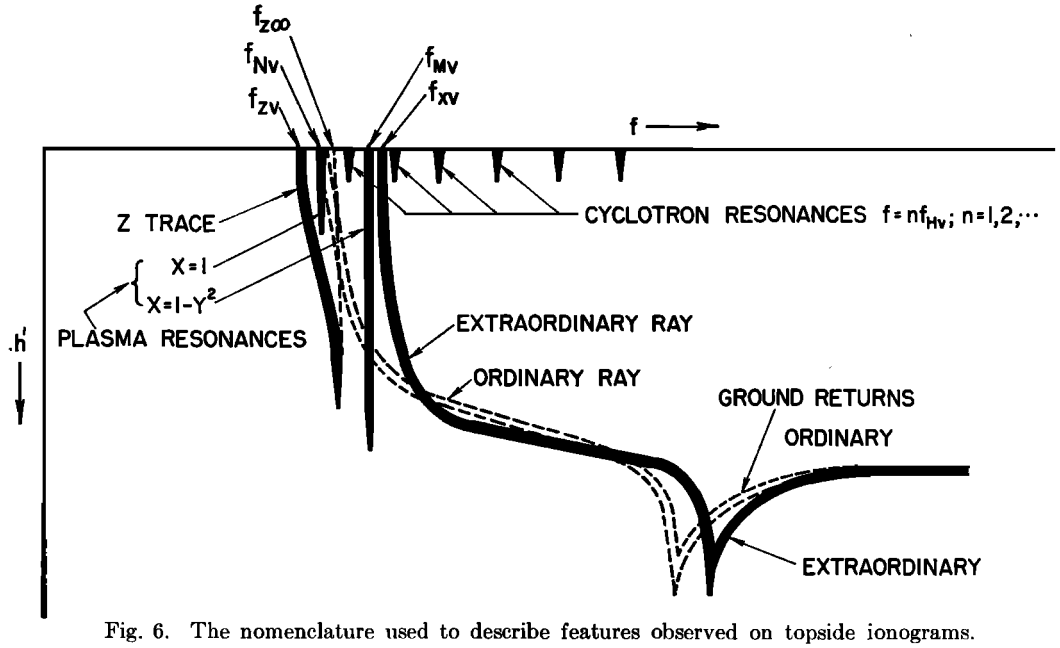

Fig. 6. The nomenclature used to describe features observed on topside ionograms.

vehicle, for f_{Hv}, the electron gyrofrequency at the vehicle, and for θ_v, the value of the dip angle at the vehicle [*Lockwood*, 1963].

Thus, for example, equation 9, giving the condition $X = 1$ for the plasma resonance (or O spike) can be used immediately to give the plasma frequency at the vehicle, since this is simply the frequency at which the plasma resonance (or O spike) is observed (Figure 6). Similarly, (7) can be used to give the value of the gyrofrequency at the vehicle from a direct measurement of the frequency at which the cyclotron harmonics are observed. These values of f_{Hv} and f_{Nv} can then be substituted into (10) to give the dip angle at the vehicle θ_v. The magnitudes of the dip angle and the gyrofrequency at the vehicle deduced as above can then be compared with the values computed by the method described in the preceding section, and an estimate can be obtained in this way of the reliability of the model used for extrapolating the observed values of the field parameters measured at the ground. In practice, either technique is sufficiently accurate for the calculation of electron densities using the procedures described below.

An inspection of the ionograms received at Stanford indicates that the extraordinary ray trace is usually the most clearly visible on the ionogram and, unlike the ordinary ray trace, the frequency at which the extraordinary ray has zero range is usually easily recognized. This

TABLE 3. Nomenclature

v	The subscript v is used to denote the value of a quantity measured at, or corresponding to, the location of the vehicle.
f	Frequency.
f_N	Plasma frequency.
f_{ov}	Frequency at which ordinary ray has zero range ($X = 1$). This is the same as the plasma frequency at the vehicle, f_{Nv}.
f_{xv}	Frequency at which extraordinary ray has zero range ($X = 1 - Y$).
f_{zv}	Frequency at which Z ray has zero range ($X = 1 + Y$).
f_{Mv}	Plasma resonance ($X = 1 - Y^2$).
f_{Nv}	Plasma resonance ($X = 1$). This is the plasma frequency at the vehicle and is the same as the frequency for the ordinary trace zero range echoes.
$f_{z\infty}$	Frequency at which Z trace has infinite virtual depth $\left(X = \dfrac{1 - Y^2}{1 - Y^2 \cos^2 (\pi/2 - \theta_v)}\right)$
f_H	Electron gyrofrequency.
f_{Hv}	Electron gyrofrequency at the vehicle.
N_v	Electron densities at the vehicle.
θ_v	Dip angle at the vehicle.
X	f_N^2/f^2.
Y	f_H/f.

TABLE 4. Relevant Magnetoionic Conditions

In this table, $X = f_N^2/f^2$, $Y = f_H/f$.

Magnetoionic Condition	Remarks	Frequency	Equation	
$Y = 1/n, \quad n = 1, 2, \cdots$	Cyclotron harmonics	nf_{Hv}	$f = nf_{Hv}$	(7)
$X = 1 + Y$	Z trace zero range echoes	f_{xv}	$f_{xv}^2 = f_{Nv}^2 - f_{xv}f_{Hv}$	(8)
$X = 1$	Ordinary trace zero range echoes	f_{ov}	$f_{ov}^2 = f_{Nv}^2$	(9)
$X = 1$	Plasma resonance	f_{Nv}		
$X = \dfrac{1 - Y^2}{1 - Y^2\cos^2(\pi/2 - \theta_v)}$	Z trace infinite range echoes	$f_{x\infty}$		(10)
$X = 1 - Y^2$	Magnetic plasma resonance	f_{Mv}	$f_{Mv}^2 = f_{Nv}^2 + f_{Hv}^2$	(11)
$X = 1 - Y$	Extraordinary trace zero range echoes	f_{xv}	$f_{xv}^2 = f_{Nv}^2 + f_{xv}f_{Hv}$	(12)

frequency (f_{xv}, Figure 6) has, accordingly, been measured and (12), corresponding to the condition $X = 1 - Y$, has been used to determine N_v, the value of the electron density at the vehicle. Thus

$$N_v = 1.24 \times 10^4 f_{Nv}^2$$
$$= (1.24 \times 10^4)(f_{xv}^2 - f_{xv}f_{Hv}) \qquad (12a)$$

where N is in electrons per cubic centimeter and f_{xv} and f_{Hv} are in megacycles per second.

In the section 'Results of the Calculations' below, the magnetic field parameters are deduced from the extrapolated ground values rather than from direct measurements on the ionograms. In this case, the electron gyrofrequency f_{Hv} is derived from the value of the total field F_v computed at the vehicle from the equation $f_{Hv} \approx 2.8F_v$, where f_{Hv} is given in megacycles per second and F_v is in gauss. F_v is calculated from F, the value of the earth's total field at the ground, by an inverse cube relation. The use of a more accurate model for the extrapolation from the value of the total field at the ground to the value at the vehicle indicates that the inverse cube extrapolation leads to errors of about 27 kc/s (i.e., about 2.5%) in the value of f_{Hv} (E. L. Hagg and G. L. Nelms, private communication).

The actual calculation of electron density at the vehicle from (12a) is performed in a digital computer. The program requires as input the frequency at which the extraordinary ray trace has zero range, f_{xv}, together with the time at which f_{xv} was observed, t_0, the pass number, and the time and longitude of the equatorial crossing for the pass concerned. The printed output from the computer gives the electron density at the vehicle, N_v, together with data about the location of the vehicle, the time of observation, the magnetic dip angle, and the electron gyrofrequency at the vehicle at the

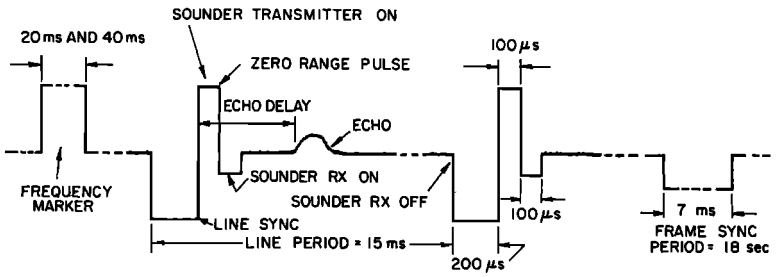

Fig. 7. Alouette video format (courtesy NASA).

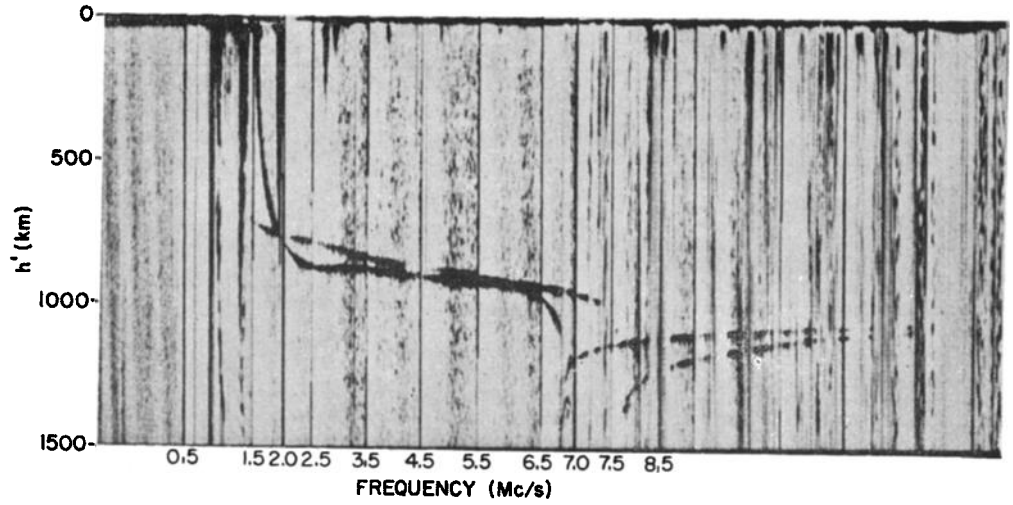

Fig. 8*a*. Example of daytime topside ionogram obtained at Stanford University. Note topside reflected rays and ground returns. The plasma resonances (or spikes) are also clearly visible, as are the cyclotron harmonics. This record was obtained at 21h 40m 03s GMT on March 15, 1963, on pass 2288, and is typical of equinoctial conditions near local noon.

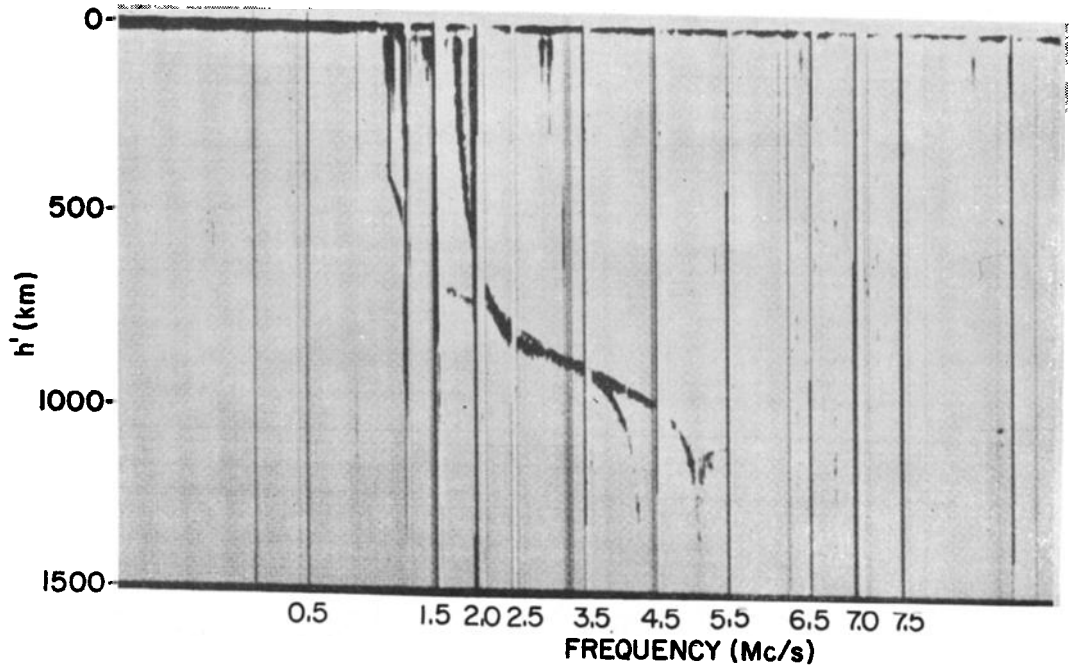

Fig. 8*b*. Example of a day-night transition-type topside ionogram observed at Stanford University. This record was obtained at 01h 16m 38s GMT on May 11, 1963, on pass 3054, and is typical of evening conditions. Note the *Z* trace.

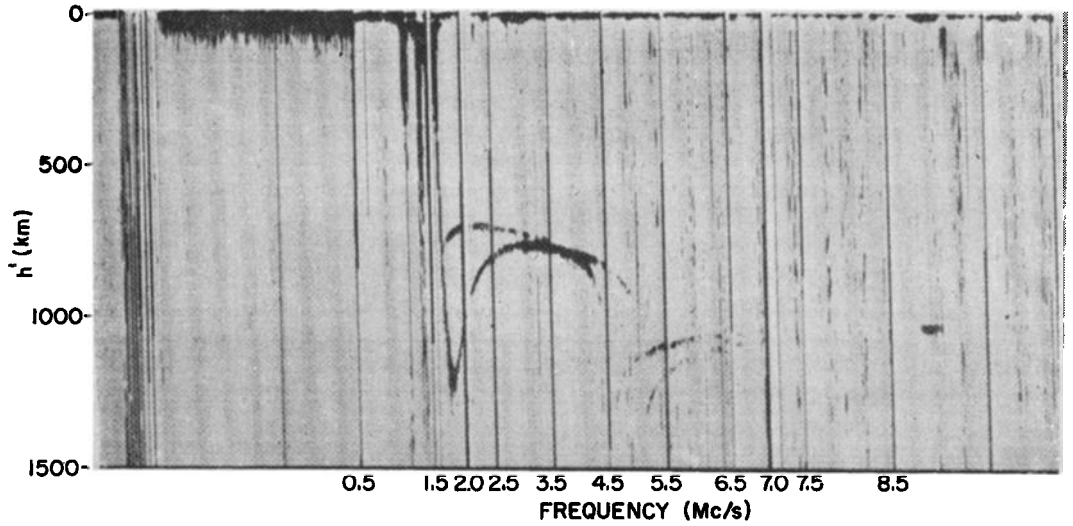

Fig. 8c. Example of nighttime ionogram observed at Stanford University. This record was obtained at 05h 23m 53s GMT on April 5, 1963, on pass 2565. Note the cusp near 1.8 Mc/s.

time concerned. The output data are obtained on magnetic tape which can be further processed so that the electron density at the vehicle, for a given pass, is automatically plotted against dip latitude (the nomenclature used is that recommended by *Chapman* [1963]) or local time at the vehicle as desired.

The result of using the outlined calculations on data from a large number of topside ionograms is presented in the section 'Results of the Calculations,' where the accuracy of the derived electron densities is also considered in detail.

Program of observations and description of typical ionograms. Ionograms from the Alouette topside sounder were recorded whenever signals from the vehicle could be acquired by the satellite monitoring facility. Two passes per day were recorded, the telemetry signals being received over a period of approximately twelve minutes per pass, so that under favorable circumstances approximately 40 ionograms could be obtained covering a range of geographic latitudes which, under the best circumstances, could extend from about 7°N to 67°N. In Figure 7 the video format used for the display of the virtual depth data is illustrated.

Typical examples of Alouette ionograms picked to show some of the main features observed are shown in Figures 8*a*, *b*, and *c*.

Results of the Calculations

Another paper [*Thomas and Westover*, 1963] describes in detail a digital computer program for converting the information contained in the reflected ray traces observed on topside ionograms into electron density profiles for the upper part of the F region; examples were given in that report of some derived topside $N(h)$ profiles. The present paper is concerned only with the calculation of the electron density at the vehicle and in particular with the determination of the diurnal, seasonal, and latitudinal variations of this quantity at the Alouette orbit.

A number of passes were selected for detailed study from the regular sequence of twice daily sets of ionograms monitored as a routine at the Radioscience Laboratory, Stanford University. The data examined were for a series of days and nights selected to correspond to summer and winter conditions in the northern hemisphere and include results for January, May, June, and July 1963 and December 1962.

Latitudinal, diurnal, and seasonal variations. In Figure 9*a* the observed midday values of f_{xv} are plotted for a series of days selected to represent summer and winter conditions as a function of dip latitude; each point represents one ionogram. In Figure 9*b* the data of Figure 9*a* have been converted into electron densities at the

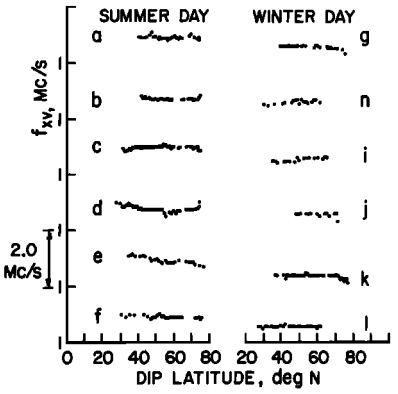

Fig. 9*a*. The variation with dip latitude of the frequency f_{xv} at which the extraordinary trace has zero range for a series of days, labeled *a–l*, in summer and in winter near local noon at the vehicle. The dates for each pass and the Greenwich mean time of the point of closest approach to Stanford of the Alouette satellite are given in Table 5.

satellite by means of (12*a*). It is clear from Figure 9*b* that during the daytime the electron density falls uniformly from low to high latitudes and it is clear also that the electron density in winter at a given latitude is lower than that in summer. These observations were made when the Greenwich mean times of the point of closest approach of the vehicle to Stanford were as shown in Table 5, so that the results of Figures 9*a* and *b* correspond roughly to local noon conditions at the vehicle. In Figure 10, the corresponding variations are shown for a series of summer and winter nights. Figure 10 shows that during the summer night the electron density reaches a minimum at a dip latitude of approximately 65°N and an examination of the curves for June 12, 13, and 14 (labeled *C, D, E,* Figure 10) also indicates the existence of a sharp local increase of electron density at a dip latitude of approximately 74°N on each night. The results for winter nights show a steady but small decrease of electron density with increasing latitude. Again, the results of Figure 10 correspond to Greenwich mean times at the vehicle which are as indicated in Table 5, so that the observations correspond to approxi-

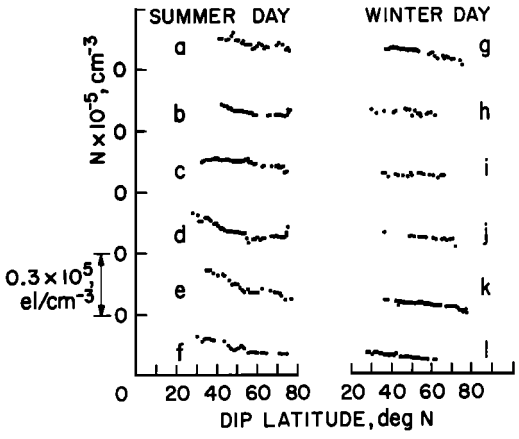

Fig. 9*b*. The variation with dip latitude of the midday electron density at 1000 km deduced from the observational data in Figure 9*a* for a series of days, labeled *a–l*, in summer and in winter. The dates for each pass and the Greenwich mean time of the point of closest approach to Stanford of the Alouette satellite are given in Table 5.

TABLE 5. Dates on Which Observations for Figures 9*a* and *b* and 10 Were Obtained

Curve	Date	GMT*
	Summer Day	
a	June 15, 1963	19.37
b	June 22	18.44
c	June 24	18.13
d	June 27	18.18
e	June 28	17.10
f	June 29	17.47
	Winter Day	
g	Dec. 21, 1962	19.03
h	Dec. 23	18.33
i	Dec. 25	18.02
j	Dec. 29	17.00
k	Dec. 30	17.38
l	Dec. 31	18.16
	Summer Night	
A	May 29, 1963	10.17
B	June 1	10.24
C	June 12	08.27
D	June 13	09 05
E	June 14	07.56
F	June 15	08 34
	Winter Night	
G	Dec. 9, 1962	09.19
H	Dec. 23	07.29
I	Dec. 24	08.07
J	Dec. 25	06.59
K	Dec. 28	07.05
L	Dec. 30	06.34

* Greenwich mean time of the point of closest approach of the satellite to Stanford.

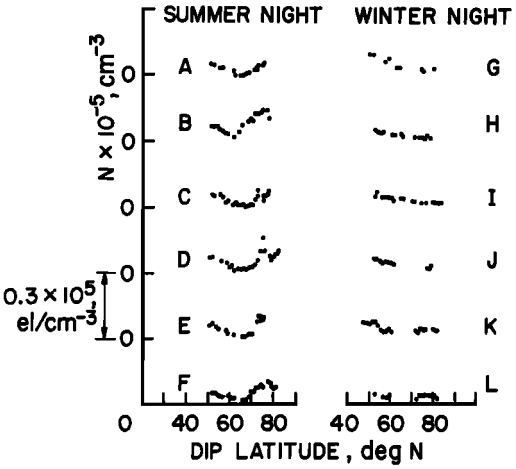

Fig. 10. The variation with dip latitude of the midnight electron density at 1000 km for a series of nights, labeled *A–L*, in summer and in winter. The dates for each pass and the Greenwich mean time of the point of closest approach to Stanford of the Alouette satellite are given in Table 5.

mately local midnight at the vehicle. Altogether 105 passes were studied; the results shown in Figures 9*a* and *b* and 10 are typical. It is quite clear that the observations repeat themselves consistently and that the Alouette experiment provides an extremely reliable and accurate technique for obtaining the electron density at 1000 km in a very simple way. Figures 9 and 10 give a sample selected at random from the 105 passes examined. In Figures 11 and 12 a mean curve has been drawn through the observations for a number of international quiet days, so that a representative variation of N_e with dip latitude is obtained for summer and winter daytime and nighttime conditions. These observations show that at the Alouette orbit the midday electron density is greater in summer than in winter throughout the latitude range over which the observations were made. The average quiet midnight electron density at 1000 km in summer shows a minimum value at a dip latitude of 65°. In a companion paper and an earlier report [*Angerami and Thomas*, 1963, 1964], these latitudinal distributions of electron density were used in a theoretical study of the distribution of electrons and ions in the earth's exosphere.

Because of the precession of the orbit, it is possible, by taking results over a long period of time, to determine the diurnal variation of the electron density at the satellite. Typical results are shown in Figure 13 in which the variation in electron density at 1000 km is given as a function of local time at the vehicle for the daytime period near noon. The electron density is plotted both for summer (circles) and for winter (dots). The results shown in Figure 13 correspond to the dip latitude range 45° to 55°N, and the individual points correspond to different days, so that the spread in these observations may arise from day-to-day variations at the vehicle. In Figure 13 a smooth line has been drawn through the points. Similar results were derived for a whole series of dip latitude ranges; these are drawn for the summer observations in Figure 14 and for the winter

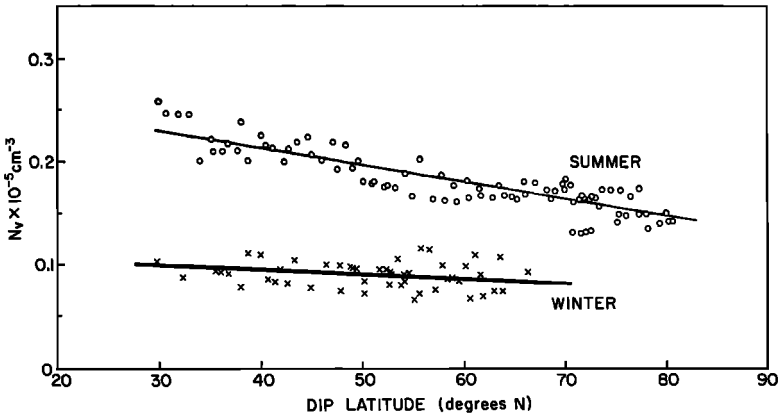

Fig. 11. The average variation with dip latitude of the electron density near noon at 1000 km for international quiet days in summer and winter. The results are for days in December 1962 and May, June, and July 1963.

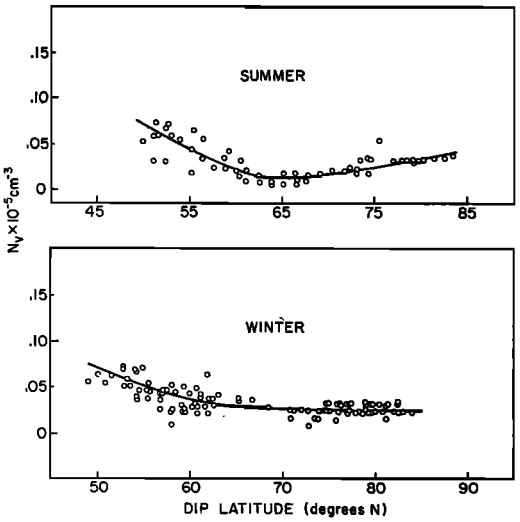

Fig. 12. The average variation with dip latitude of the electron density near midnight at 1000 km for international quiet days in summer and winter. The results are for days in December 1962 and January, May, June, and July 1963.

observations in Figure 15. It is interesting to compare the results illustrated in these two figures. Figure 14 shows that the diurnal variation is not the same at different latitudes and that the time at which the maximum electron density at 1000 km is reached depends on the dip latitude. At high latitudes the peak occurs about half an hour after noon, whereas at low latitudes it occurs about one and a half hours after noon. It seems likely that such a variation would arise from a variation of temperature with latitude.

The decrease in electron density at a given time with increasing latitude is also shown in Figures 14 and 15. We see that the general level of electron density over a given geomagnetic latitude range is lower in winter than it is in summer and that in a given geomagnetic latitude range the electron density in summer can be approximately twice that in winter. The winter observations do not show the marked increase in electron density that occurs after noon in the summer observations, although there is again evidence that the maximum is reached later in the afternoon at low latitudes than it is at high latitudes. Typical daytime electron densities in summer at 1000 km at noon during 1963 are of the order of 15,000 to 20,000 electrons/cc, and perhaps as many as 30,000 to 40,000 electrons/cc at very low latitudes. In winter at noon the number of electrons varied from about 8000 to 10,000/cc. The electron densities in the nighttime ionosphere at about 1000 km for both summer and winter are shown in Figure 16. An examination of the nighttime electron densities observed over a series of latitude ranges indicates that after midnight there is no strong dependence of the nocturnal N_v variation on latitude, and it is therefore convenient to present all the results over the latitude range 45° to 75°N magnetic in one diagram, Figure 16. We see that the electron density at 1000 km shows considerable variation from

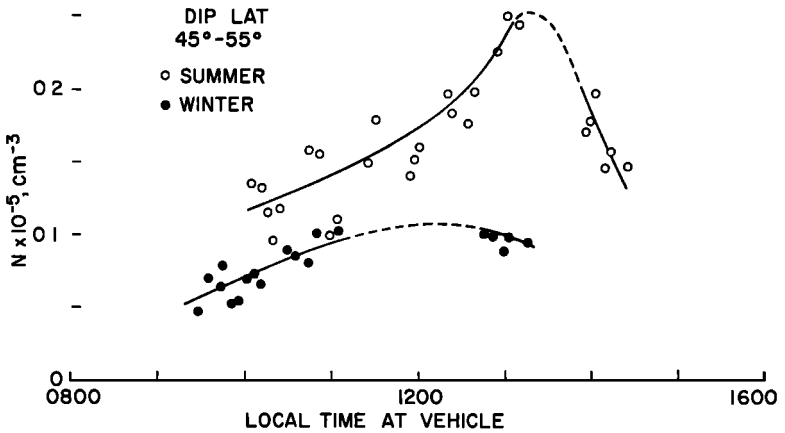

Fig. 13. The variation with local time at the vehicle near noon of the electron density at 1000 km over the range of dip latitudes 45° to 55°N for a series of days in summer (circles) and in winter (dots).

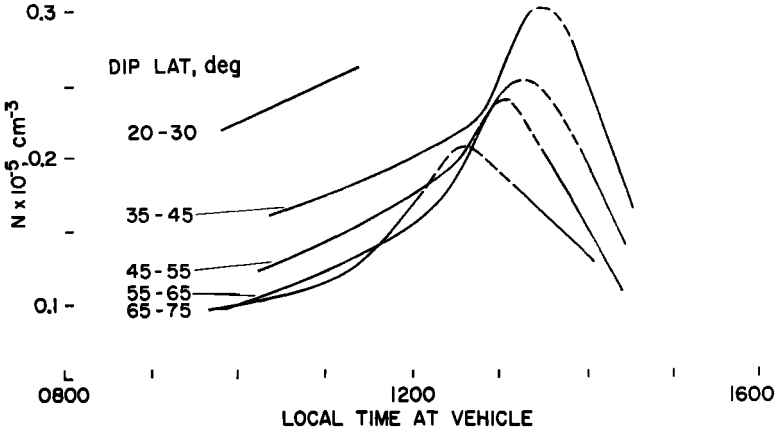

Fig. 14. The variation with local time at the vehicle during the day of electron density at 1000 km for a series of latitude ranges in summer 1963.

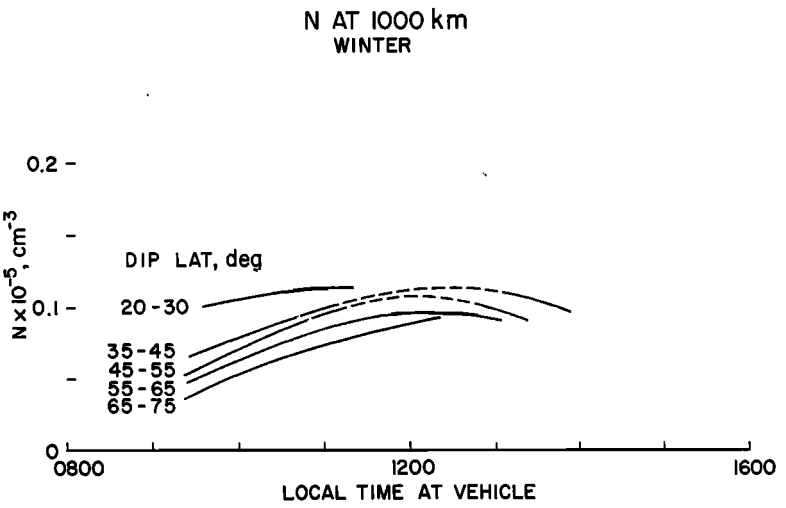

Fig. 15. The variation with local time at the vehicle during the day of electron density at 1000 km for a series of latitude ranges in winter 1962–1963.

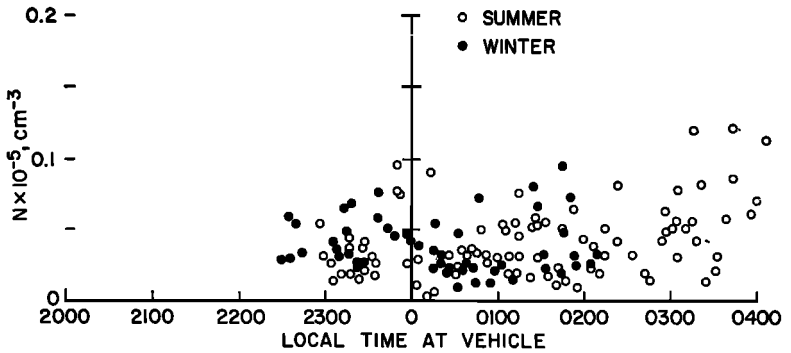

Fig. 16. The nighttime electron density at 1000 km over the range 45° to 75°N geomagnetic latitude in summer (circles) and in winter (dots) as a function of local time at the vehicle for 1962–1963.

night to night, with electron densities at midnight ranging from 1000/cc to 10,000/cc, 5000/cc being the mean value.

Accuracy of observations. The absolute error ΔN_v in N_v, the electron density at the vehicle computed from (12*a*), is given by

$$\Delta N_v = 1.24 \times 10^4 \Delta(f_{Nv}^2)$$
$$= 1.24 \times 10^4 \Delta f_{xv}(2f_{xv} - f_{Hv}) \qquad (13)$$

where Δf_{xv} is the error in measurement of the quantity f_{xv}. The relative error is

$$\Delta N_v/N_v = \Delta f_{xv}\left[\frac{1}{(f_{xv} - f_{Hv})} + \frac{1}{f_{xv}}\right] \qquad (14)$$

It is clear that the magnitude of the error in f_{Nv} and hence in N_v depends on the magnitude of the observed quantity f_{xv} and on the accuracy to which it can be measured (±0.05 Mc/s). During the daytime when f_{xv} is relatively large, the error in electron density derived using (12*a*) is negligibly small. However, as the electron density at the vehicle falls from its daytime to its nighttime value and as f_{xv} approaches the electron gyrofrequency f_{Hv}, it is clear that the electron density at the vehicle will then be computed from the difference of two small and almost equal quantities, namely, f_{xv}^2 and $f_{Hv}f_{xv}$, and the absolute and relative errors in N_v become large. Under these circumstances, it may be best, for the nighttime observations, to compute the electron density at the vehicle not from f_{xv}, but from the plasma resonance corresponding to the condition $X = 1$. It should be noted, however, that the use of the extraordinary ray frequency f_{xv} permits the measurement of electron densities lower than that corresponding to a plasma frequency equal to the lowest frequency transmitted by Alouette (~0.5 Mc/s corresponding to $N_v \approx 3000$/cc). For example, if $f_{Hv} = 0.5$ Mc/s and f_{xv} is just observable, say, at 0.6 Mc/s, then $N_v \approx 750$/cc, which is the approximate lower limit of electron density detectable by Alouette. The magnitude of the error in N_v resulting from the use of (12*a*) has been computed from (13) and (14) and is shown in Table 6 for different assumed values of f_{Hv} for $\Delta f_{xv} = 0.05$ Mc/s. It is clear that the technique using the extraordinary trace becomes less accurate for very low values of f_{xv}, and the error (Table 6) becomes greater than 10% when $f_{xv} - f_{Hv}$ is less than about 0.8 Mc/s. Thus it is likely that nighttime electron densities are less accurately determined than daytime values. However, as can be seen from Table 6, except under the circumstances just outlined, the electron density at the vehicle can be determined from (12*a*) to an accuracy of better than ±10%. Thus, apart from the need for caution when using the extraordinary trace when the electron density at the vehicle is low, the technique described in this report offers a very simple and accurate way of determining the electron density at the Alouette orbit and its variations with time.

TABLE 6. Magnitude of Error in N_v

f_{Hv}, Mc/s	N_v, el/cc	f_{xv}, Mc/s	ΔN_v	$\Delta N_v/N_v$, %
0.6	40000.0	2.121	2258.0	5.6
	35000.0	2.007	2116.2	6.0
	30000.0	1.884	1964.3	6.5
	25000.0	1.751	1799.6	7.2
	20000.0	1.605	1618.1	8.1
	15000.0	1.440	1413.6	9.4
	10000.0	1.247	1174.0	11.7
	5000.0	1.002	870.9	17.4
0.8	40000.0	2.240	2281.7	5.7
	35000.0	2.127	2141.5	6.1
	30000.0	2.006	1991.5	6.6
	25000.0	1.875	1829.2	7.3
	20000.0	1.732	1651.1	8.3
	15000.0	1.570	1451.2	9.7
	10000.0	1.383	1219.0	12.2
	5000.0	1.150	930.6	18.6
1.0	40000.0	2.364	2311.8	5.8
	35000.0	2.253	2173.6	6.2
	30000.0	2.134	2025.9	6.8
	25000.0	2.005	1866.7	7.5
	20000.0	1.865	1692.5	8.5
	15000.0	1.708	1498.1	10.0
	10000.0	1.528	1274.5	12.7
	5000.0	1.308	1002.2	20.0
1.2	40000.0	2.494	2348.1	5.9
	35000.0	2.384	2212.1	6.3
	30000.0	2.267	2067.3	6.9
	25000.0	2.141	1911.4	7.6
	20000.0	2.005	1741.7	8.7
	15000.0	1.853	1553.6	10.4
	10000.0	1.680	1339.2	13.4
	5000.0	1.474	1083.3	21.7

Conclusions

It has been shown that a measurement of the frequency at which the extraordinary ray trace observed on topside ionograms has zero range

provides a rapid and accurate technique for determining the electron density at the Alouette satellite. The calculation requires a knowledge of the dip angle and the gyrofrequency for electrons at the vehicle. These can be derived from extrapolated values of the earth's field as measured at the ground (if the position of the satellite at a given time is known accurately) or from observations on the ionograms themselves. Techniques for calculating the position of the satellite from accurate positional data determined from the Alouette orbital data were described.

Using these techniques, the latitudinal, diurnal, and seasonal variations of the electron density at the Alouette orbit have been determined for conditions representative of summer and winter daytime and nighttime periods. It is observed that the electron density at ~1000 km varies from nighttime minimum values of approximately 1000 electrons/cc to daytime maximum values likely to be reached near the magnetic equator of about 40,000 electrons/cc. The electron density falls steadily from low latitudes to high latitudes and is greater in summer than in winter by a factor of the order of 2. The summer daytime variations in electron density at the vehicle are interesting in that they show that the maximum value of electron density at this level is reached much later in the afternoon at low latitudes than it is at high latitudes for the data analyzed.

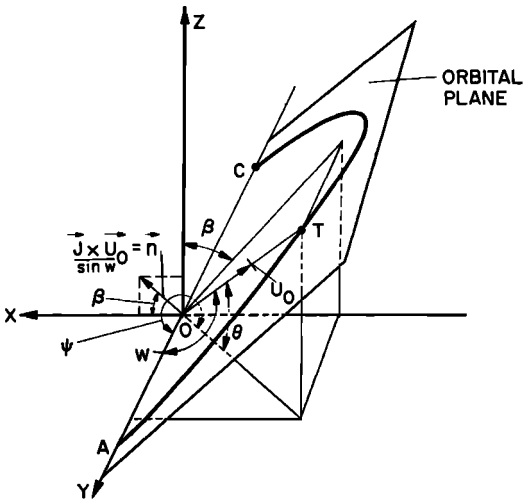

Fig. 17. The trajectory of the Alouette satellite over a latitude range of 10° is assumed to be in the plane ATC.

Appendix A

Calculation of Latitude and Longitude of Subsatellite Point

It is assumed that the orbital trajectory of the Alouette satellite is planar over the latitude range of 10° considered below. Since the orbit is almost circular, so that the distance from the center of the earth is almost constant, the trajectory in this plane could be defined as a function $\Psi = f(w)$, where w is the azimuth in the orbital plane ATC, and Ψ is the angle (measured clockwise) from the equatorial crossing point to the point corresponding to the projection of the satellite on to the plane of the equator (Figure 17). If OA coincides with the Greenwich meridian, Ψ is the longitude measured in degrees west of Greenwich. T is the subsatellite point, and can be represented by the coordinates (w, θ) or (Ψ, θ). In accordance with Kepler's laws, the area swept out by the radius vector to the satellite during unit time is proportional to the azimuth w. The longitudes (determined from tables similar to Table 4 of *Thomas and Sader* [1963]) for the crossing points of the 10° latitude-longitude network used for calculating the position of the subsatellite point correspond to projections from the plane of the orbit on to the equatorial plane. In the calculations described, linear interpolations in time using these longitudes are made. If the interpolation had been carried out over the curved path of the Alouette orbit, a slightly different and more accurate longitude would have been derived for the subsatellite point. The magnitude of the error is evaluated below.

From the orbital elements, the inclination of the plane orbit is known to be 80.464°, so that the complement β of this angle (Figure 17) is 9.536°. Consider the rectangular coordinate system $OXYZ$ defined in the plane of the equator, OY corresponding to the direction of a south-north equatorial crossing of the satellite. The equation of the orbital plane in this coordinate system (Figure 17) is

$$\frac{X}{Z} = -\tan \beta \qquad \text{(A.1)}$$

For the same system in spherical coordinates, a

unit vector **U** taken along **R** will have the components

$$\mathbf{U} = \frac{X}{\rho}\mathbf{i} + \frac{Y}{\rho}\mathbf{j} + \frac{Z}{\rho}\mathbf{k}$$

where

$$\mathbf{R} = X\mathbf{i} + Y\mathbf{j} + Z\mathbf{k} = \rho\mathbf{U}$$

and **i**, **j**, and **k** are unit vectors along OX, OY, and OZ, respectively; ρ is the distance from the origin to the point concerned (OT); and θ is the angle between the plane OXY and the line OT (Figure 17).

For the same system in spherical coordinates, the components of **U** along OX, OY, OZ, will be, respectively, $\cos\theta \sin\Psi$, $\cos\theta \cos\Psi$, and $\sin\theta$.

If the coordinates of the unit vector **U** are to satisfy (A.1), then

$$\mathbf{U}_0 \cdot \mathbf{j} = \cos w \qquad \text{(A.2)}$$

$$\mathbf{U}_0 \times \mathbf{j} = -\mathbf{n} \sin w \qquad \text{(A.3)}$$

where **n** has the components $\cos\beta$, 0, $\sin\beta$, respectively, and $\mathbf{U}_0$ now lies in the orbital plane. Equations A.2 and A.3, expressed with respect to the components in rectangular coordinates, yield

$$\cos w = \cos\theta \cos\Psi \qquad \text{(A.4)}$$

$$\mathbf{U}_0 \times \mathbf{j} = \begin{vmatrix} \mathbf{i} & \mathbf{j} & \mathbf{k} \\ \cos\theta \sin\Psi & \cos\theta \cos\Psi & \sin\theta \\ 0 & 1 & 0 \end{vmatrix}$$

Thus,

$$\sin\theta = \sin w \cos\beta \qquad \text{(A.5)}$$

$$\cos\theta \sin\Psi = -\sin\beta \sin w \qquad \text{(A.6)}$$

Using (A.4) and (A.5)

$$\Psi = 2\pi - \arctan \sin\beta \tan w$$

$$= f(w) \quad \text{say} \qquad \text{(A.7)}$$

$$w = \arcsin(\sin\theta / \cos\beta) \qquad \text{(A.8)}$$

The error in longitude has been computed for Alouette ($\beta = 9.536°$) for a series of ranges of latitudes. The results are shown in Table 7. Ψ was computed for steps of 1° in θ from (A.7) and (A.8), and is given in Table 7 in the column labeled Ψ (computed). In addition, linear interpolation has been made in these computed values of Ψ at integral multiples of 10°. The resulting values of Ψ (interpolated) for the middle of each latitude range are also shown in this table. The difference Ψ (computed) $-$ Ψ (interpolated) is always positive and gives the maximum error in longitude that can arise over the particular interval of latitude concerned. This quantity is shown in the last column of Table 7.

The interpolated longitudes are too small by an amount which does not exceed the value shown in the last column of Table 7, and it is clear that except for very high latitudes the error due to using a linear interpolation in the determination of longitude is small.

Tables 5 and 6 of the paper by *Thomas and Sader* [1963] show that the differences at the end points of the 2° grid network of the values of total field and dip angle near 70° latitude are of the order of 0.001 gauss and 0.5°, respectively. Thus, for the range of latitudes relevant to the observations described in this report, even if the maximum possible error in the computed longitude were to occur, the resulting change in the values of f_{H_e} and θ_e required in the computation of the electron density at the vehicle would be negligible.

A similar error arises in the calculation of the latitude of the vehicle. This error can be calculated by a similar procedure using $\theta = f(w) = \arcsin(\sin w \cos\beta)$ where the angles are, as before, given in Figure 17 (see equation A.7).

TABLE 7. Error in the Calculation of Longitude

Geographic Latitude, deg	Latitude at Midinterval, h, deg	Ψ (computed), deg	Ψ (interpolated), deg	Maximum Error, deg
0–30	25	355.51	355.46	0.05
30–40	35	353.24	353.17	0.07
40–50	45	350.33	350.17	0.16
50–60	55	346.12	345.77	0.35
60–70	65	338.88	337.80	1.08

An evaluation of the magnitude of this error in latitude shows that it is even smaller than that computed above for longitudes, since the plane of the orbit is highly inclined to the equatorial plane.

Appendix B

Interpolation in Curvilinear Coordinates—The Derivation of Equation 6

Let z be a scalar parameter defining the magnetic field at the subsatellite point T (Figure 18). Let L and M be the curvilinear coordinates of the point T on the sphere representing the earth. The origin for this coordinate system is taken as the point D in the grid network $ABCD$ of spacing 2°. L is thus the length measured along the parallel at the latitude through T from the meridian through BD having a west longitude ϕ. M is the length measured along the meridian through T from the parallel at latitude θ. The corresponding coordinates referred to the intersection of the Greenwich meridian and the plane of the equator as origin are denoted by l and m, respectively, so that

$$l_1 < l < l_2 \qquad m_1 < m < m_2$$

where l_1 and l_2 are consecutive values of the longitude grid lines, and m_1 and m_2 consecutive values of the latitude grid lines (Figure 18). It should be noted that l_1, l_2, m_1, m_2, l, and m, refer to lengths along the sphere and not to the corresponding angles, which are ϕ_1, ϕ_2, θ_1, θ_2, ϕ, and θ, respectively (Figure 18).

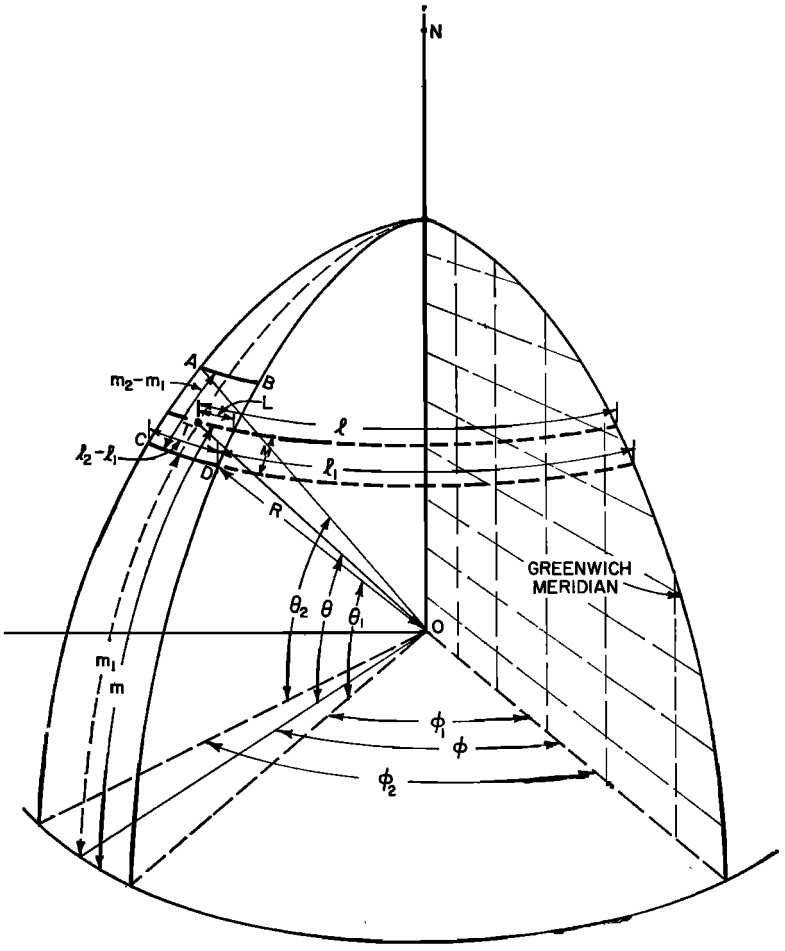

Fig. 18. The curvilinear coordinate system used in the derivation of (6).

Suppose that at the corners of the grid network $ABCD$ (Figures 5 and 18), the magnetic field parameter z has the values z_1 at D, z_2 at C, and z_3 at B. Developing the function $G(l, m) = z$ around the point D (Figure 18), the total differential of z is given by

$$dz = \frac{\delta z}{\delta l}\, dl + \frac{\delta z}{\delta m}\, dm \qquad \text{(B.1)}$$

We have

$$\delta l = l_2 - l_1 = Rk(\phi_2 - \phi_1) \cos \theta_1$$

where $k = \pi/180$ and R is the radius of the earth. Thus

$$\frac{\delta z}{\delta l} = \frac{z_3 - z_1}{Rk(\phi_2 - \phi_1) \cos \theta_1}$$

$$= \frac{q}{Rk(x_2 - x_1) \cos \theta_1} \qquad \text{(B.2)}$$

Similarly

$$\frac{\delta z}{\delta m} = \frac{z_2 - z_1}{Rk(\theta_2 - \theta_1)} = \frac{p}{Rk(y_2 - y_1)} \qquad \text{(B.3)}$$

where p, q, x_1, x_2, y_1, and y_2 are as previously defined. We have

$$L = dl = l - l_1 = Rk(x - x_1) \cos \theta$$

$$dm = m - m_1 = Rk(y - y_1)$$

where θ is the latitude of the point T. Substituting (B.2) and (B.3) in (B.1), the value of the magnetic field parameter at the subsatellite point T is given by

$$z - z_1 = p\, \frac{(x - x_1) \cos \theta}{(x_2 - x_1) \cos \theta_1} + q\, \frac{(y - y_1)}{(y_2 - y_1)}$$

$$z = \frac{\cos \theta}{\cos \theta_1}\, \frac{X}{a}\, p + \frac{Y}{b}\, q + z_1$$

which is the previously quoted (6).

Acknowledgments. We acknowledge gratefully the courtesy of scientists of the Canadian Defence Research Telecommunications Establishment, Ottawa, Canada, particularly Dr. J. H. Chapman and Dr. G. L. Nelms, who provided a number of topside ionograms in the early stages of this work. We also thank Dr. J. H. Chapman of the Canadian Defence Research Telecommunications Establishment and Mr. J. E. Jackson of the Goddard Space Flight Center, National Aeronautics and Space Administration, for permission to monitor signals from the Alouette satellite at Stanford. The telemetry receiving station at Stanford has been operated by Messrs. S. Hall, D. Annett, and K. Byram. It is a pleasure to acknowledge the efforts of all these contributors to the program.

The work was financed by grant NsG 30-60 from the National Aeronautics and Space Administration and was carried out while one of us (Dr. J. O. Thomas) was a Visiting Scientist at the Radioscience Laboratory, Stanford University.

The interest of Professors O. G. Villard, Jr., and O. K. Garriott of the Radioscience Laboratory is gratefully acknowledged.

References

Angerami, J. J., and J. O. Thomas, The distribution of ions and electrons in the earth's exosphere, *Tech. Rept. 4, grant NsG 30-60* and *AF-AFOSR-62-370, Stanford Electron. Lab., Stanford Univ.*, 1963.

Angerami, J. J., and J. O. Thomas, Studies of planetary atmospheres, 1, The distribution of electrons and ions in the earth's exosphere, *J. Geophys. Res., 69*(19), October 1, 1964.

Calvert, W., and G. B. Goe, Plasma resonances in the upper ionosphere, *J. Geophys. Res., 68,* 6113, 1963.

Canadian Defence Research Telecommunications Establishment, *Alouette, Satellite 1962 Beta Alpha One,* Canadian Defence Research Board, Ottawa, 1962.

Chapman, S., Geomagnetic nomenclature, *J. Geophys. Res., 68,* 1174, 1963.

Hagg, E. L., A preliminary study of the electron density at 1000 kilometers, *Can. J. Phys., 41,* 195, 1963.

Hydrographic Office (now the Navy Oceanographic Office), The total intensity of the earth's magnetic field for the year 1955, *Map 1703, 2nd edition,* Navy Oceanographic Office, Washington, D. C., December 1954*a*.

Hydrographic Office (now the Navy Oceanographic Office), The magnetic inclination or dip angle for the year 1955, *Map 1700, 7th edition,* Navy Oceanographic Office, Washington, D. C., December 1954*b*.

Lockwood, G. E. K., Plasma and cyclotron spike phenomena observed in topside ionograms, *Can. J. Phys., 41,* 190, 1963.

Nelms, G. L., Scale heights of the upper ionosphere from topside soundings, *Can. J. Phys., 41,* 202, 1963.

Petrie, L. E., Topside spread echoes, *Can. J. Phys., 41,* 194, 1963.

Thomas, J. O., A. R. Long, and D. E. Westover, The calculation of electron density profiles from topside sounder records, *J. Geophys. Res., 68,* 3237, 1963.

Thomas, J. O., and A. Y. Sader, Alouette topside soundings monitored at Stanford University, *Tech. Rept. 6, grant NsG 30-60, Stanford Electron. Lab., Stanford Univ.*, 1963.

Thomas, J. O., and D. E. Westover, The calculation of electron density profiles from topside

ionograms using a digital computer, *Tech. Rept. 5, grant NsG 30-60, Stanford Electron Lab., Stanford Univ.*, 1963.

Warren, E. S., Sweep frequency radio soundings of the topside of the ionosphere, *Can. J. Phys., 40*, 1692, 1962.

Warren, E. S., Perturbation of the local electron density by Alouette satellite, *Can. J. Phys., 41*, 188, 1963*a*.

Warren, E. S., Some preliminary results of sounding of the topside of the ionosphere by radio pulses from a satellite, *Nature, 197*, 636, 1963*b*.

(Manuscript received July 13, 1964.)